A00-36710

AIAA-00-3520

Progress in Development of a Combined Device/Plume Model for Hall Thrusters

I. D. Boyd, L. Garrigues, J. Koo, M. Keidar
University of Michigan
Ann Arbor, MI 48109.

PROGRESS IN DEVELOPMENT OF A COMBINED DEVICE/PLUME MODEL FOR HALL THRUSTERS

Iain D. Boyd*, Laurent Garrigues§, Justin Koo‡ and Michael Keidar†

University of Michigan, Ann Arbor, MI 48109

Abstract

Two different numerical techniques are employed to model the plasma flow in the acceleration channel and plume of a Hall thruster. The models are applied to the SPT-100 Hall thruster due to the availability of experimental data. A hybrid, Monte Carlo Collision-Particle in Cell approach is employed to model the unsteady flow in the acceleration channel. Time averaged velocity distribution functions from the device model are used as input into the steady flow plume model that employs a hybrid, direct simulation Monte Carlo–Particle in Cell method. Results for thruster performance and plume properties are compared with available experimental data. These comparisons suggest the sensitivity of the device model to the magnetic field configuration.

Introduction

Development of computational models to accurately predict the plasma properties in the acceleration channel and plume of a Hall thruster is required for several reasons. In terms of the device plasma, an accurate model could be used in the design of thrusters with improved performance. In addition, models could be used to predict erosion on the channel walls that represents the primary lifetime limiting mechanism. A detailed model describing the plasma jet is required for assessment of spacecraft integration concerns such as sputtering and charging of solar arrays, and deposition of material sputtered from the channel walls.

Computer models describing the plasma flow in Hall thrusters have been developed by Komurasaki and Arakawa,[1] Fife,[2] and Boeuf and Garrigues.[3] In Ref. 1, a steady state, two-dimensional, kinetic formulation was employed. In Refs. 2 and 3, an unsteady formulation was employed consisting of the fluid equations for the electrons, and a particle approach for the heavy species. The work described here represents a combination of the approaches adopted in Refs. 2 and 3. We have chosen to study the SPT-100 Hall thruster as this device has been studied in detail experimentally, and is the most well known Hall thruster.

Computer models of Hall thruster plumes have been developed by Oh and Hastings,[4] VanGilder et al.,[5], and Boyd.[6] A review of Hall thruster modeling activities has been presented recently by Boyd.[7] The models described in Refs. 4-6 again use particle methods for the heavy species, and the Boltzmann fluid relation for the electrons. This approach is again used in the present work.

* Associate Professor. Department of Aerospace Engineering. Senior Member AIAA.

§ Research scientist. Department of Aerospace Engineering. Permanent address: CPAT, Toulouse, France.

‡ Graduate student research assistant. Department of Aerospace Engineering.

† Research scientist. Department of Aerospace Engineering.

One of the main conclusions of Ref. 7 is the need to combine in a seamless fashion the modeling activities for the Hall thruster device and its plume. The main reason for this is that the plume computations generally employ measured performance data such as the thrust, mass flow rate, and current, together with assumptions about the various species temperatures and the beam divergence, to estimate the thruster exit properties. This is perhaps an acceptable engineering approach, but is not at all satisfactory in terms of trying to develop a predictive capability. This problem had been recognized several years ago,[8] but until now had not been addressed. The approach adopted in our work is to use velocity distribution functions computed at the thruster exit by the acceleration channel model as input into the plume model. In the following, we first describe the device plasma model. This is followed by a brief description of the plume model. A variety of results are then presented for the SPT-100 Hall thruster. These include thruster performance over a range of operating conditions, thruster exit profiles, and plume properties. Wherever possible, comparisons are made with existing experimental data.

Hybrid-MCC-PIC Device Model

The axially symmetric model (z,r) is based on a combination of some of the general assumptions employed in an earlier one-dimensional model of Boeuf and Garrigues[3], together with many of the ideas proposed by Fife.[2] A fluid description is used for the transport of the electrons, which are assumed to follow a Maxwellian velocity distribution. A particle approach is used for the heavy particles (ions and neutrals). Under normal operating conditions of the SPT-100 (applied voltage of 300 V and a flow rate of 5 mg/s of xenon), the double charge ion current represents typically 10% of the total ion current, and so for this study, its influence is neglected. In the first part of this section, the particle approach for the heavy species is described. In the second part, the electron transport is described. Finally, the calculation of the magnetic field shape is discussed.

A. Particle Approach for Heavy Species

1. Ion transport

Since the ion mean free path is larger than the size of the thruster, the ions are assumed to be collisionless in the channel. Moreover, an estimate of the Larmor radius of the ions at the thruster exit (where the magnetic field strength is about 200 G and the ion velocity is about 1.6×10^4 m/s) gives a value of about 1 m. Thus it is reasonable to neglect the influence of the magnetic field on the ion transport.

The computational domain is divided into cells (typically 30x30 in the present calculations). Standard Particle-In-Cell (PIC)[9] algorithms are employed that allow full control over the total number of particles in the domain through use of macro-particles. In each computational cell, a population of ion particles is created by the following source term due to the ionization:

$$S(\mathbf{r}) = n_e(\mathbf{r}) n_a(\mathbf{r}) k_i(\mathbf{r}) \tag{1}$$

where n_e is the electron density (set equal to the ion density using the assumption of quasineutrality), n_a is the neutral atom density, k_i is the ionization rate, and $\mathbf{r}$ is the vector position. The initial velocity of the

ions is sampled from a Maxwellian distribution function at a temperature of 1000 K. Then the equations of motion of the ions are integrated using a leap-frog scheme. The time step Δt is chosen small enough that high-energy ions stay in the same cell for several iterations during their transport.

All the trajectories of the sample of macro-particles are integrated until the ions arrive at the exit of the thruster, or return to the injector. Any ions reaching the walls or the surfaces below and above the injector are eliminated; new neutrals are created to take into account the recombination. The velocity of new neutral particles is also determined according to a Maxwellian distribution function with a temperature equal to that of the injector (1000 K). The ion density is calculated on the nodes of the grid by computing the weight of the macro-particles at the four corners of the cell occupied by each particle. With the assumption of quasineutrality, the plasma density is deduced directly from the ion density.

2. Neutral atom transport

The same macro-particle method is used for the neutral atoms as for the ion transport. The neutral particles are introduced into the computational domain at the injector. In most Hall thrusters, the neutral gas is injected into the channel through a number of holes uniformly distributed around the circumference of the anode. To introduce the mass flow rate uniformly, the number of apertures in the distributor can vary from a few tens to one hundred. To simplify the injection of neutral particles in the computation, a continuous annular opening is considered with an inner radius of 3.8 cm and an outer radius of 4.2 cm. The initial positions of the particles introduced at the injector is determined randomly, and their velocities are distributed with a half-Maxwellian distribution function based on a temperature of 1000 K. The trajectories of the neutrals are integrated in the same manner as for the ions with no electric force. All neutrals leaving the domain (across the exit and injector planes) are eliminated. A neutral macro-particle reaching the wall, or the plane below and above the injector, is scattered back into the domain. No energy losses are assumed on the wall. A Monte Carlo Collision (MCC) method[10] is used to take into account the loss of neutrals due to ionization. During the integration of the neutral trajectory, a probability of collision is calculated using

$$P = n_i(\mathbf{r}) k_i(\mathbf{r}) \Delta t \tag{2}$$

For the plasma of the SPT-100, the condition $P << 1$ always holds. An accept-reject method is used to decide if the neutral should be eliminated from the simulation due to ionization. The scheme used to compute the neutral density on the nodes of the grid is the same as that for the ions. The number of neutral macro-particles in the simulation fluctuates from 60,000 during periods of high current to 80,000 during periods of low current.

B. Fluid Description of Electron Transport

We are primarily interested in the time scales related to the heavy species, which are typically two or three orders of magnitude higher than the electron transport time scale. Thus, we consider the steady state fluid equations of electron transport.

1. Momentum Equation Along Magnetic Field Lines

Due to the configuration of the magnetic field, the electron transport is greater in the azimuthal direction (Hall current) than in the axial direction (drift diffusion due to collisions). The electron transport along magnetic field lines can be written as a balance between the pressure force and the electric force

$$\frac{\partial(en_e kT_e)}{\partial \mathbf{r}_{\|}} = en_e \frac{\partial V}{\partial \mathbf{r}_{\|}} \tag{3}$$

where n_e and T_e are respectively the electron density and temperature, k is the Boltzmann constant, V is the electric potential and $\mathbf{r}_{\|}$ is the distance vector along the magnetic field lines. This assumption may be less valid in the anode region where the strength of the magnetic field is small. Assuming a constant electron temperature along the magnetic field lines, we obtain

$$V - \frac{kT_e}{e} ln(n_e) = constant \tag{4}$$

The electric potential is constant along the magnetic field lines and relation (4) can be written as:

$$V - \frac{kT_e}{e} ln\left(\frac{n_e}{n_{e,0}}\right) = V^*(\lambda) \tag{5}$$

where V^* is constant along a magnetic field line and $n_{e,0}$ is the reference electron density at the reference plasma potential V_0 set to 0. Note that V^* is sometimes referred to in the Russian literature as a *thermalized potential*.[11] The gradient of the magnetic stream function λ is everywhere orthogonal to the magnetic field such that:[2]

$$\frac{\partial \lambda}{\partial z} = rB_r \tag{6a}$$

$$\frac{\partial \lambda}{\partial r} = -rB_z \tag{6b}$$

Equation (5) makes it possible to reduce the two-dimensional calculation of the electric field to a one-dimensional problem.

2. Momentum Equation Across Magnetic Field Lines

For the electron momentum equation in the direction normal to the magnetic field lines, the electron current can be written as a sum of drift and diffusion terms assuming an isotropic pressure tensor

$$J_{e,\perp} = -en_e \mu_{e,\perp} E_\perp - eD_{e,\perp} \frac{\partial n_e}{\partial \mathbf{r}_\perp} \tag{7}$$

where $E_\perp$, $\mu_{e,\perp}$, and $D_{e,\perp}$ are the electric field, the electron mobility and the electron diffusion terms in the direction across the magnetic field, and $\mathbf{r}_\perp$ is the distance vector normal to the magnetic field lines. The coefficients $\mu_{e,\perp}$ and $D_{e,\perp}$ are linked by the Einstein relation

$$\frac{D_{e,\perp}}{\mu_{e,\perp}} = \frac{kT_e}{e} \tag{8}$$

In the calculations, $\frac{D_{e,\perp}}{\mu_{e,\perp}}$ is set to a constant corresponding to a mean value of the electron temperature in the anode region (in the first 5 mm) where the electron temperature profile is flat.

Differentiation of Eq. (6) in the direction normal to the magnetic field, using $\mathbf{E} = -\nabla V$ and assuming that $\frac{kT_e}{e}$ is constant, we obtain:

$$J_{e,\perp} = -en_e\mu_{e,\perp}rB\frac{\partial V^*}{\partial \lambda} \tag{9}$$

where B is the magnitude of the magnetic field. The electron mobility in the direction normal to the magnetic lines is assumed to be the classical collision mobility

$$\mu_{e,\perp} = \frac{e}{m\nu_m}\frac{1}{1+\frac{\omega_{c,e}^2}{\nu_m^2}} \tag{10}$$

where m is the electron mass, $\omega_{c,e}$ is the electron angular cyclotron frequency and ν_m is the total electron momentum exchange collision frequency. This collision frequency is the sum of a term due to electron-neutral collisions and a term due to electron-wall scattering. Electrons can diffuse across magnetic field lines due to collisions with neutrals and with the walls of the channel (which can play the same role as a collision with an atom: the so-called "near-wall conductivity"). As in the 1D model of Ref. 3

$$\nu_m = (\nu_m)_{neutrals} + (\nu_m)_{walls} \tag{11}$$

where

$$(\nu_m)_{neutrals} = k_m n_a \tag{12}$$

with k_m=2.5 $\times$ 10^{-7} cm^{-3} s^{-1}.

The electron-wall collision frequency is assumed to be constant throughout the channel, and given by $(\nu_m)_{walls} = \alpha_w \times 10^7$ s^{-1} where α_w is a parameter. It was found in Ref. 3 that experimental values of current were reasonably well reproduced by the 1D model for α_w=0.2, and the same value is again used here.

3. Continuity equation

The current conservation equation can be written as

$$I_T = I_e + I_i \tag{13}$$

where I_e is the electron current and I_i is the ion current. Note that in the model developed by Fife,[2] a near wall electron current is added to take into account the effect of secondary electron emission on the electron transport. Writing Eq. (13) in an integral form along the magnetic field line:

$$I_T = \int_0^l 2\pi en_e\mu_{e,\perp}r^2B\frac{\partial V^*}{\partial \lambda}dl + \int_0^l 2\pi en_i u_{i,\perp}rdl \tag{14}$$

where $u_{i,\perp}$ is the ion velocity normal to the B lines, and dl is a length of an element along the magnetic field line. The electric field can be deduced from the relation above in terms of the total current, the plasma density n_p (=n_e=n_i), the ion normal velocity $u_{i,\perp}$, the electron mobility $\mu_{e,\perp}$ and the magnetic field B

$$E(\lambda) = \frac{I_T - \int_0^l 2\pi en_p u_{i,\perp}rdl}{\int_0^l 2\pi en_p\mu_{e,\perp}r^2Bdl} \tag{15}$$

The potential drop V_{max} is imposed and we can express the electric field in terms of the applied potential using the relation

$$V_{max} = -\int_0^d E(\lambda)d\lambda \tag{16}$$

to obtain the total current. No external circuit is taken into account. The plasma density and the ion normal velocities are calculated by integrating the ion properties (density and normal flux) between two elements of the λ grid. Knowing the total current, the electric field is then calculated on the λ grid using Eq. (15) by imposing the potential drop between the center of the anode and the center of the exit plane. The profile of the electric field makes it possible to deduce the thermalized potential, V^*, on the λ grid (right term of the relation (14)). The electric potential in the entire domain is then calculated by inverting Eq. (14) and the electric field obtained from $\mathbf{E}=-\nabla V$.

4. Energy equation

The electron temperature is supposed constant along the magnetic field lines; thus a one-dimensional equation is used for the electron energy with variations in the axial direction only. The steady state energy equation can be written as follows:

$$\frac{\partial}{\partial x}\left(\frac{5}{3}n_e \mathrm{v}_{e,\perp}\varepsilon_e + q_{e,\perp}\right) = -en_e \mathrm{v}_{e,\perp}E_\perp - n_e\varepsilon_e\nu(\varepsilon_e) \tag{17}$$

where ε_e is the electron mean energy, $\nu(\varepsilon_e)$ is the total electron energy loss frequency, and $E_\perp$ is the mean radial value of the axial electric field. The thermal flux is approximated by

$$q_{e,\perp} = -\frac{2}{3}\kappa_{e,\perp}\frac{\partial\varepsilon_e}{\partial x} = -\frac{5}{3}n_e D_{e,\perp}\frac{\partial\varepsilon_e}{\partial x} \tag{18}$$

The total electron energy loss frequency $\nu(\varepsilon_e)$ depends on a term due to the inelastic electron-neutral collisions and a contribution due to the effect of the secondary electron emission by electron impact. The different inelastic collision terms are calculated assuming a Maxwellian distribution function for the electrons. The secondary electron emission coefficient is higher than 1 for values of incident electrons energy around 20-30 eV. Electrons that have energy higher than this threshold lose energy extracting low energy electrons from the surface of the walls. This effect tends to limit the electron energy in the channel. An empirical formula used to describe the inelastic losses at the wall by high-energy electrons employed in the previous 1D model is again used here:

$$\nu(\varepsilon_e)_{wall} = \alpha_w 10^7 exp\left(-\frac{U}{\varepsilon_e}\right) \tag{19}$$

where U is a parameter taken to be equal to 20 eV in the calculations, and α_w is the same as above.

The electron energy equation is integrated by inverting a tridiagonal matrix and estimating the total electron energy loss frequency using the energy of the previous time step. The electron energy boundary conditions consist of fixing the electron mean energy in the exit plane at 10 eV and imposing a zero slope condition at the anode plane.

C. Magnetic Field Configuration

Here we follow an approach similar to that proposed by Fife.[2] In the real device, electro-magnets and polar pieces form the magnetic circuit. The position of the polar pieces plays a major role to maintain a strong radial component of the magnetic field in the exit region of the device. The shape and the strength of the magnetic field are changed by varying the current passing through the magnets. This current comes from a separate power supply in laboratory Hall thruster or by connecting the magnets in series with the discharge current for flight models. To permit a study on the effect of the magnetic field lines on the plasma properties and on the performance, we have chosen to use the magnetic field as a parameter. In the channel, we have

$$\nabla \times \mathbf{B} = 0$$

This allows the introduction of a scalar magnetic potential, V_m:

$$\mathbf{B} = -\nabla V_m$$

where V_m satisfies Laplace's equation. A radial magnetic field profile is imposed on the walls of the SPT and a magnetic axial profile on the anode and exit planes. Laplace's equation is then solved in cylindrical coordinates using a Successive Over Relaxation (SOR) method. To compute the magnetic field shape, a grid of 50x50 points is employed. The magnetic field is then calculated on the nodes of the MCC-PIC grid by interpolation.

Hybrid-DSMC-PIC Plume Model

The Hall thruster plume model uses a steady, hybrid (fluid–particle) approach. Ions are tracked as particles using the Particle-In-Cell method.[9] The plasma potential is obtained by assuming quasi-neutrality allowing the total ion density to be equated to the electron density. By representing electrons as a fluid and further assuming that they are isothermal, collisionless, and un-magnetized, the Boltzmann relation is invoked:

$$n_e = n_{ref} exp\left(\frac{\phi}{kT_e}\right) \tag{20}$$

where n_e is the electron number density, n_{ref} is a reference density where the potential ϕ is zero, k is Boltzmann's constant, and T_e is the constant electron temperature. Inversion of Eq. (20) gives the potential that is then differentiated spatially to obtain the electric fields.

There are several limitations of the Boltzmann relation approach. Firstly, experimental evidence[12] indicates that there is variation of the electron temperature in Hall thruster plumes. The variation occurs mainly in the near-field of the plume. At the thruster exit the electron temperature can be as high as 10 eV[12] and in the far field typical values are 1 to 2 eV. This creates a difficulty in the choice of T_e to be used in Eq. (19). A further difficulty with application of the Boltzmann relation to Hall thruster plumes is the possible effects of the magnetic field. The combination of permanent and electro-magnets employed in

Hall thrusters are designed to provide optimum device performance. However, some of the magnetic field may leak out into the plume of the thruster. The amount of this leakage will depend strongly on the Hall thruster type and configuration.

Collisions involving heavy particles are simulated using the direct simulation Monte Carlo (DSMC) method.[13] This involves collecting groups of particles into cells that have sizes of the order of a mean free path. Pairs of these particles are then selected at random and a collision probability is evaluated for each pair that is proportional to the product of the pair's relative velocity and collision cross section. The probability is compared with a random number to determine if that collision occurs. If so, some form of collision dynamics is performed to alter the properties of the colliding particles. There are three basic classes of collisions that may occur in Hall thruster plumes: (1) elastic; (2) charge exchange; and (3) Coulomb.

Elastic collisions involve only exchange of momentum between the participating particles. For the systems of interest here, this may involve atom–atom or atom-ion collisions. For atom–atom collisions, the Variable Hard Sphere (VHS)[13] collision model is employed. For the high energy atom–ion elastic interactions involved in the Hall thruster plume, we employ the model of Dalgarno et al..[14] The collision dynamics assumes isotropic scattering together with conservation of linear momentum and energy to determine the post-collision velocities of the colliding particles.[13]

Charge exchange concerns the transfer of one or more electrons between an atom and an ion. In the present work, we use the cross section for Xe-Xe^+ measured recently by Pullins et al.[15] as follows:

$$\sigma_{CEX}(Xe, Xe^+) = (142.21 - 23.30 log_{10}(g)) \times 10^{-20} \mathrm{m}^2 \tag{21}$$

where g is the relative velocity of the collision. In Ref. 15, the charge exchange cross section for Xe-Xe^{2+} was also measured and found to be approximately half of that for Xe-Xe^+. In all charge exchange collisions, the collision dynamics assumes that there is no transfer of momentum accompanying the transfer of the electron(s).

Coulomb interactions involve collisions between charged species (ion-ion, electron-ion, and electron-electron). These collisions have been neglected in Hall thruster plume modeling mainly because the cross sections are only significant for very small scattering angle interactions. This has been confirmed for xenon flow through an ion thruster in which the inclusion of Coulomb collisions in a PIC-DSMC model were found to have no effect on the computed properties.[16]

Results

As mentioned earlier, we have chosen to study the SPT-100 Hall thruster mainly because of the availability of a significant amount of experimental data for this device. However, it is important to state clearly what is meant here by the SPT-100. Development of this thruster continues in several countries. The general dimensions of these SPT-100 thrusters are similar. We consider the acceleration channel to have a length of 25 mm and be defined between diameters of 60 and 100 mm. Unfortunately, the magnetic field configurations of different SPT-100's are not the same, and in some cases their acceleration channel wall materials

are different. In all cases, the magnetic field configuration is withheld for proprietary reasons. This makes our modeling activity difficult. We have chosen a relatively simple magnetic configuration that we believe to be *representative* of that found in a real device. However, the hybrid-MCC-PIC results are very sensitive to the magnetic field employed and we do not claim to make an exact comparison between the model and the measured data for the same thruster. The radial magnetic field configuration employed in the results presented in this study is shown in Fig. 1 and was computed using the procedure outlined earlier. It is expected that the field in a real SPT-100 would have more curvature and less symmetry about the channel center line. In some ways, the field we have assumed is likely to give enhanced performance in comparison to the fields achieved in real devices.

Using the magnetic field shown in Fig. 1, the unsteady hybrid-MCC-PIC results for the flow will be first presented and discussed. Time-averaged velocity distribution functions in the thruster exit plane obtained from these calculations form the input for the hybrid-DSMC-PIC model of the plume.

Hall Thruster Device

The standard operational conditions considered are a mass flow rate of 5 mg/s, an applied voltage of 300 V, and a total current of 4.5 A. We estimate that the fall in potential between the external cathode and the thruster exit plane is 25 V. This means that in the case of an applied voltage of 300 V, the device only sees a voltage drop of 275 V between the anode and the thruster exit plane. For this case, the current oscillates with a frequency of about 24 kHz as shown in Fig. 2. This is very close to the value of 26 kHz measured for the SPT-100 by Ohler et al..[17] Of course, all of the plasma properties in the channel are oscillating, including the thrust as shown in Fig. 3.

Figures 4a–4c show contours of plasma density at three points in time during a half-cycle of a typical oscillation. In Fig. 4a, the plasma density is shown at the peak of the wave. As we proceed through Figs. 4b and 4c, the rapid decrease in the plasma density is clearly shown. The location of the peak of the plasma density does not change, but it's magnitude decreases by a factor of about four. The corresponding contours for the neutral atom density are shown in Figs. 5a–5c. These show much less variation than the results for the plasma density. The variation along the channel centerline of the plasma and neutral densities obtained from Figs. 4 and 5 are shown in Figs. 6a and 6b, respectively. The plasma density profiles in Fig. 6a show the half-cycle decrease as expected. It is interesting to note that the neutral density contours do not definitively show a minimum at the time when the plasma density is a maximum. The explanation offered by Boeuf and Garrigues[3] for the oscillations in the Hall thruster involves a breathing mechanism in which the neutral atoms are consumed by ionization until they reach a critically low level. Then, until they are replenished, the ionization, and hence the current is reduced. The present results support this explanation, although it is difficult to see, and the correlation between the ion density and the neutral density is much weaker in our two-dimensional results than those obtained in the prior one-dimensional investigation.[3]

The time-averaged thrust as a function of applied voltage obtained from the model is shown in Fig. 7 where comparison to measured performance[18] is included. The code over predicts the thrust by about 10%

for all cases. Contours of time-averaged plasma potential are shown in Fig. 8. Comparison with the contours of plasma density shown in Figs. 4 indicates that the ions are primarily formed in a region of very high potential. The over prediction of thrust indicates that in the real thruster, the plasma potential probably decays a little more rapidly than the simulation results. These effects may be explained in part by the lack of exact knowledge of the magnetic field. However, there are also many aspects of the numerical modeling that need to be improved such as the electron drift across magnetic field lines, and the near-wall conductivity.

It is of interest to consider the flow properties at the thruster exit as these will be employed as input boundary conditions to the hybrid-DSMC-PIC plume model. The time-averaged velocity distributions of ions and atoms in three-dimensions are the input required by the plume model. We have evaluated several different moments of these distributions and some of the results are shown in Figs. 9a-9d. The number densities of xenon ions and atoms are shown in Fig. 9a. The ions reach a maximum density of about 4×10^{11} cm^{-3} at the center of the channel and decay significantly towards the walls due to recombination. The maximum atom densities are at the walls with values of about 1.5×10^{12} cm^{-3}. The axial velocities of the ions and neutrals are compared in Fig. 9b. In both cases the profiles are almost flat with the ions at about 19 km/s and the atoms at about 350 m/s. The ion velocity is about 10% higher than that expected from reported values of the specific impulse for the SPT-100 and this is consistent with the thrust results shown in Fig. 7. The neutral velocity is close to the sonic speed for a temperature of 1000 K. The radial velocity profiles are shown in Fig. 9c. There is a small degree of asymmetry in the profiles with a larger peak velocity magnitude above the centerline of the channel. The decrease in the magnitude of the radial velocity at each of the walls is a result of the electric fields there approaching zero. These fields are determined by the pressure gradients along the magnetic field lines and these gradients become close to zero at the walls. Future studies will consider the effect of including a sheath model along the walls. Taking the peak axial and radial velocities gives an expected beam divergence angle of about 7.5°. This is smaller than the values of 10-20° that were assumed in previous Hall thruster plume computations.[5,6] Finally, the ion temperatures in the axial and radial directions are shown in Fig. 9d. These temperatures are computed as the second moment of the velocity distribution functions:

$$T = \frac{m}{k}(< u^2 > - < u >^2) \tag{22}$$

and therefore provide a measure of the spread of the distribution. The model clearly predicts that the radial velocity distribution is significantly narrower than that for the axial velocity components.

Hall Thruster Plume

The hybrid-DSMC-PIC computation is performed in a computational domain that extends 1.1 m axially from the thruster and 1.1 m radially from the plume centerline. The plume expands into a a finite back pressure of 0.006 Pa that corresponds to the experiments of King.[19] A constant electron temperature of 3 eV is used in the Boltzmann relation. The time-averaged velocity distributions from the hybrid-MCC-PIC code are employed directly as input to the plume model, and not the integrated information shown in Figs. 9.

Contours of ion density computed in the plume are shown in Fig. 10. The thruster exit plane has an axial coordinate of zero. These contours show the expected behavior with a rapid decrease in plasma density away from the axis.

The radial component of the ion velocity at 11 mm from the thruster exit is shown in Fig. 11. The measurements are due to Manzella[20] and the comparison again indicates that the device model predicts lower radial ion velocities than occur in the real thruster. In Figs. 12a and 12b, radial profiles of ion current density in the plume near field at axial distances of 10 mm and 50 mm from the thruster are shown. The experimental data are due to Kim et al..[12] These comparisons indicate that there are processes in the near field that are not presently captured by the plume model. The work of VanGilder et al.[5] suggest that this structure requires inclusion of the variation of electron temperature in the near field plume modeling.

Now, the far field plume expansion region is considered. In Figs. 13a and 13b, angular profiles of ion current density are shown at distances of 50 cm and 100 cm, respectively. The experimental data was obtained by King.[19] It is clear that the computed profiles predict a significantly narrower plume than that produced by the real thruster. The peak density on the centerline predicted by the model is significantly higher than that measured, and the large-angle values computed by the model are less than those measured experimentally. This behavior is consistent with the device model over predicting the axial velocity and under predicting the radial velocity.

Finally, in Fig. 14, the computed ion energy distribution function is compared to the measured data of King[19] on the plume axis at a distance of 50 cm from the thruster. These results indicate again that the device model over predicts the axial velocity (by about 10%). However, this comparison also indicates that the prediction of ion axial temperatures of several ten's of eV at the thruster exit is correct. There is a failure in the plume model to produce the high energy structure measured experimentally. There has been some debate about the source of this structure with the possibility that it arises due to instrument effects.

Summary

A modeling approach for simulating Hall thrusters from inside the acceleration channel to the plume far field has been developed and applied to the SPT-100 device. The system uses a hybrid-MCC-PIC method to model the unsteady, two-dimensional flow in the acceleration channel. A key aspect of the device computations involves the magnetic field configuration. This is often changed for different versions of the SPT-100 and in all cases the configuration is kept secret for proprietary reasons. In the present study, a magnetic field has been employed that is representative of the type of field employed in the real device. Low frequency oscillations with a frequency of about 24 kHz were simulated by the model. Time-averaged results for thrust were about 10% higher than experimental measurements. The code predicted ion temperatures at the thruster exit of 10–40 eV in the axial direction and about 1 eV in the radial direction. Time-averaged velocity distributions were calculated and then used as input for a hybrid-DSMC-PIC model of the Hall thruster plasma plume.

The DSMC-PIC results were compared with several different types of experimental data. These comparisons indicated that the MCC-PIC device model over predicted the ion axial velocity and under predicted the ion radial velocity. These inaccuracies may be in part due to the inability to prescribe the actual magnetic field employed in the SPT-100. In addition, there is the requirement to include Xe^{2+} in the device model.

The combination of MCC-PIC for the thruster and DSMC-PIC for the plume offers a unique capability for analyzing Hall thrusters. The long-term goal of this work is to develop computer models that can play a significant role in the design and assessment of new devices. The results presented here represent a first important step in this direction.

References

[1] Komurasaki, K. and Arakawa, Y., "Two-Dimensional Numerical Model of Plasma Flow in a Hall Thruster," *Journal of Propulsion and Power*, Vol. 11, 1995, pp. 1317-1323.

[2] Fife, J. M., "Hybrid-PIC Modeling and Electrostatic Probe Survey of Hall Thrusters," Doctoral Thesis, Massachusetts Institute of Technology, Department of Aeronautics and Astronautics, September 1998.

[3] Boeuf, J.-P. and Garrigues, L., "Low Frequency Oscillations In a Stationary Plasma Thruster," *Journal of Applied Physics*, Vol. 84, 1998, pp. 3541-3554.

[4] Oh, D. Y., Hastings, D. E., Marrese, C. M., Haas, J. M., and Gallimore, A. D., "Modeling of Stationary Plasma Thruster-100 Thruster Plumes and Implications for Satellite Design," *Journal of Propulsion and Power*, Vol. 15, 1999, pp. 345-357.

[5] VanGilder, D.B., Boyd, I.D., and Keidar, M., "Particle Simularions of a Hall Thruster Plume," *Journal of Spacecraft and Rockets*, Vol. 37, 2000, pp. 129-136.

[6] Boyd, I.D., "Computation of the Plume of an Anode Layer Hall Thruster," to appear in *Journal of Propulsion and Power*, July 2000.

[7] Boyd, I. D., "A Review of Hall Thruster Plume Modeling," AIAA Paper 2000-0466, January 2000.

[8] Qarnain, S. and Martinez-Sanchez, M., "Issues Regarding the Generation of an End-to-End Hall Thruster Computational Model," AIAA Paper 98-3796, July 1998.

[9] Birdsall, C. K. and Langdon, A. B., *Plasma Physics Via Computer Simulation*, Adam Hilger Press, 1991.

[10] Birdsall, C. K., "Particle-in-Cell Charged-Particle Simulations, Plus Monte Carlo Collisions With Neutral Atoms," *IEEE Transactions on Plasm Physics*, Vol. 19, 1991, pp. 65-85.

[11] Morozov, A. I., Esipchuk, Yu. V., Tilinin, G. N., Trofimov, A. V., Sharov, Yu. A., Shchepkin, G. Ya., "Plasma Accelerator With Closed Electron Drift and Extended Acceleration Zone," *Soviet Journal of Plasma Physics*, Vol. 17, 1972, p. 38.

[12] Kim, S., Foster, J. E., and Gallimore, A. D., "Very Near-Field Plume Study of a 1.35 kW SPT-100," AIAA Paper 96-2972, July 1996.

[13] Bird, G. A., *Molecular Gas Dynamics and the Direct Simulation of Gas Flows*, Oxford University Press, Oxford, 1994.

[14] Dalgarno, A., McDowell, M. R. C., and Williams, A., "The Mobilities of Ions in Unlike Gases," *Proceedings of the Royal Society*, Vol. 250, April 1958, pp. 411-425.

[15] Pullins, S., Chiu, Y., Levandier, D, and Dressler, R., "Ion Dynamics in Hall Effect and Ion Thrusters: Xe^+ + Xe Symmetric Charge Transfer," AIAA Paper 00-0603, January 2000.

[16] Crofton, M. W. and Boyd, I. D., "The Origins of Accelerator Grid Current: Analysis of T5-Grid Test Results," AIAA Paper 99-2443, June 1999.

[17] Ohler, S. G., Gilchrist, B. E., and Gallimore, A. D., "Electromagnetic Signal Modification in a Localized High-Speed Plasma Flow: Simulations and Experimental Validation of a Stationary Plasma Thruster (SPT)," *IEEE Transactions on Plasma Science*, Vol. 27, No. 2, 1999, pp. 587-593.

[18] Bechu, S., Perot, C., Gascon, N., Lasgorceix, P., Hauser, A. and Dudeck, M., "Operating Mode Investigation of a Laboratory Stationary Plasma Thruster," AIAA paper 99-2567, July 1999.

[19] King, L. B., "Transport-Property and Mass Spectral Measurements in the Plasma Exhaust Plume of a Hall-Effect Space Propulsion System," Doctoral Thesis, University of Michigan, Department of Aerospace Engineering, May 1998.

[20] Manzella, D. H., "Stationary Plasma Thruster Ion Velocity Distribution," AIAA Paper 94-3141, July 1994.

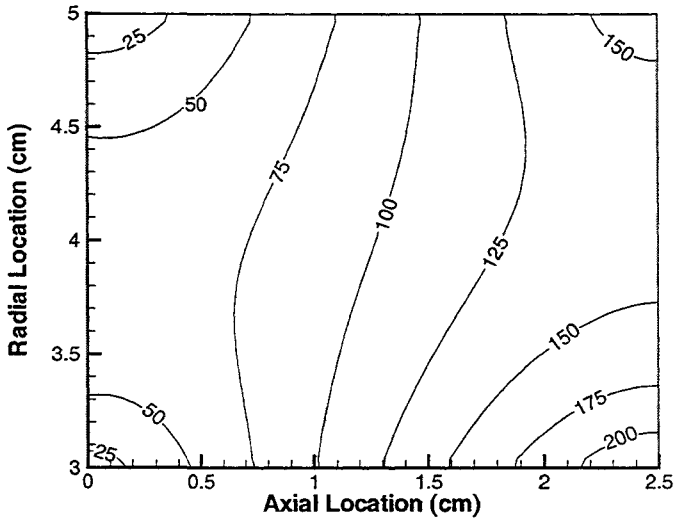

Fig. 1. Radial magnetic field configuration (Gauss) used in the hybrid-MCC-PIC computations.

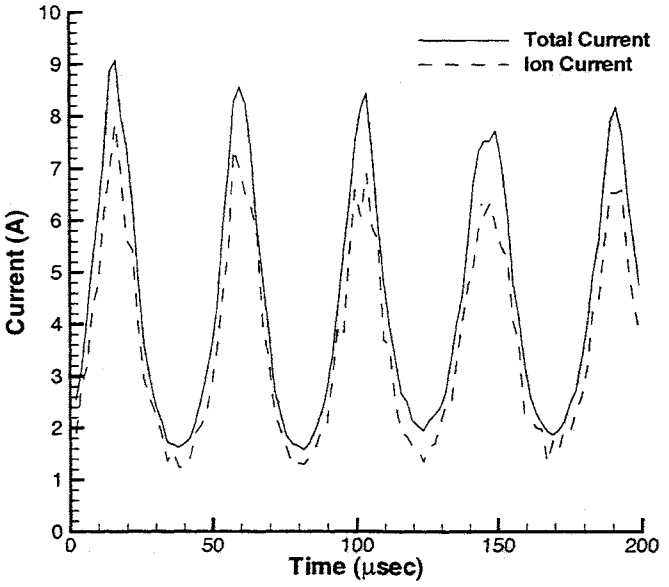

Fig. 2. Oscillating current predicted by the hybrid-MCC-PIC device model: applied voltage of 300 V, and a flow rate of 5 mg/s.

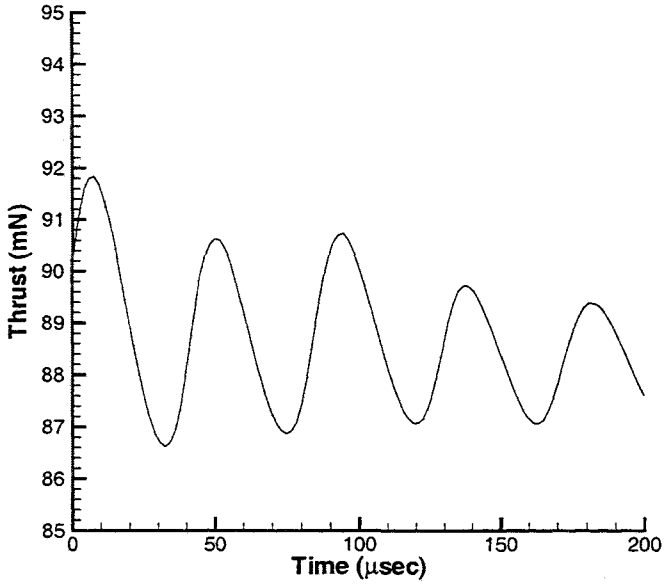

Fig. 3. Oscillating total thrust predicted by the hybrid-MCC-PIC device model: applied voltage of 300 V, and a flow rate of 5 mg/s.

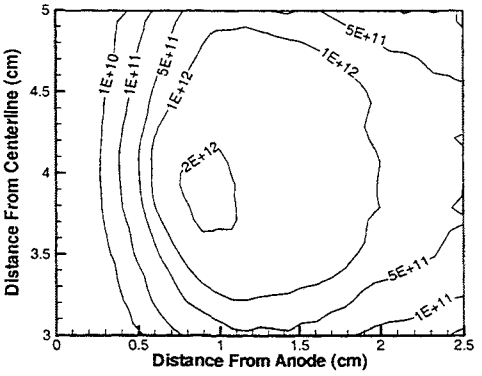

Fig. 4a. Plasma density (cm^{-3}) at a current wave peak.

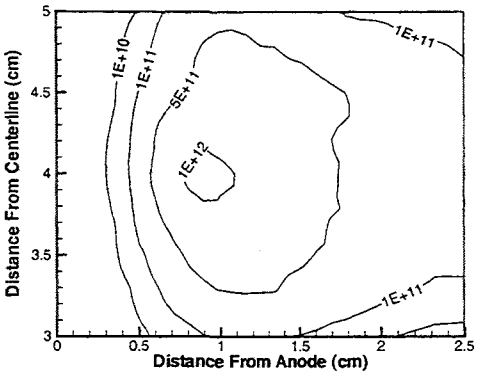

Fig. 4b. Plasma density (cm^{-3}) at 11 μsec after the current wave peak.

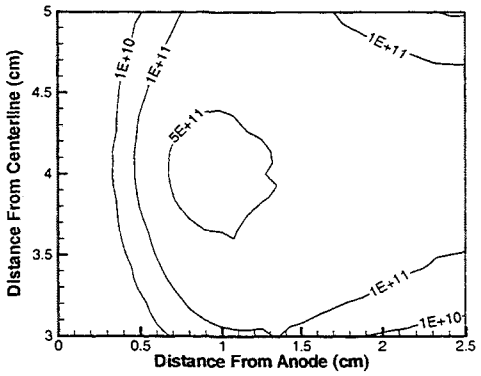

Fig. 4c. Plasma density (cm^{-3}) at 22 μsec after the current wave peak.

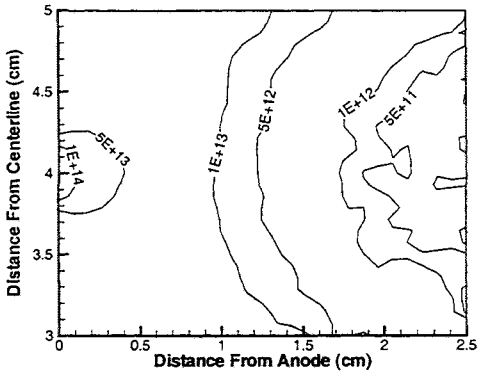

Fig. 5a. Neutral density (cm^{-3}) at the current wave peak.

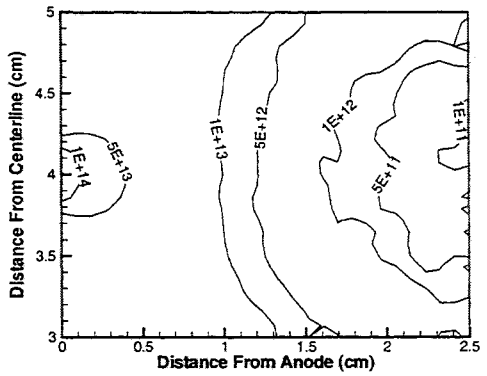

Fig. 5b. Neutral density (cm^{-3}) at 11 μsec after the current wave peak.

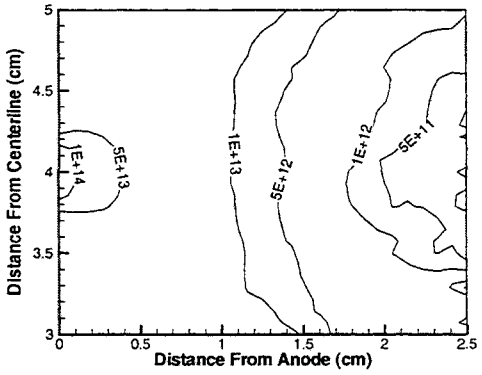

Fig. 5c. Neutral density (cm^{-3}) at 22 μsec after the current wave peak.

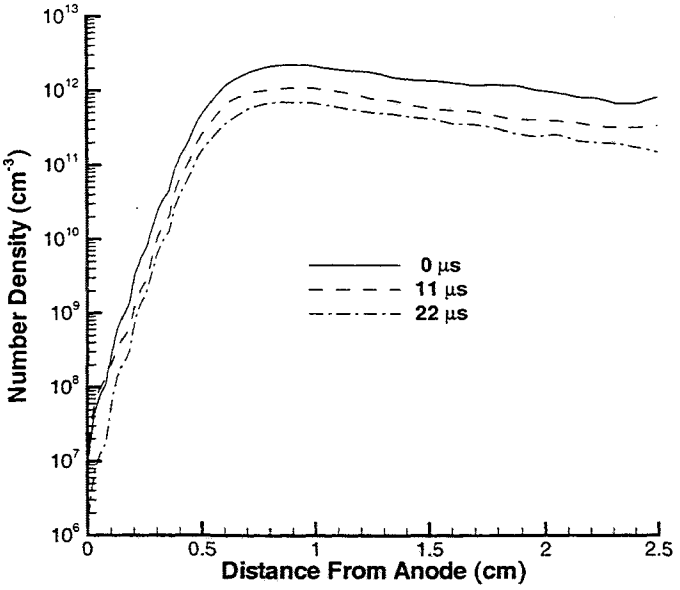

Fig. 6a. Plasma density along the channel centerline at three different times in a current oscillation wave.

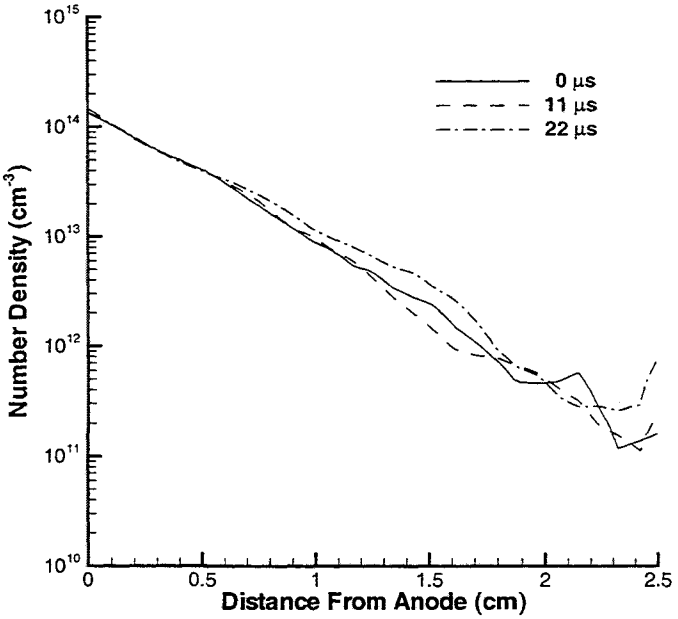

Fig. 6b. Neutral density along the channel centerline at three different times in a current oscillation wave.

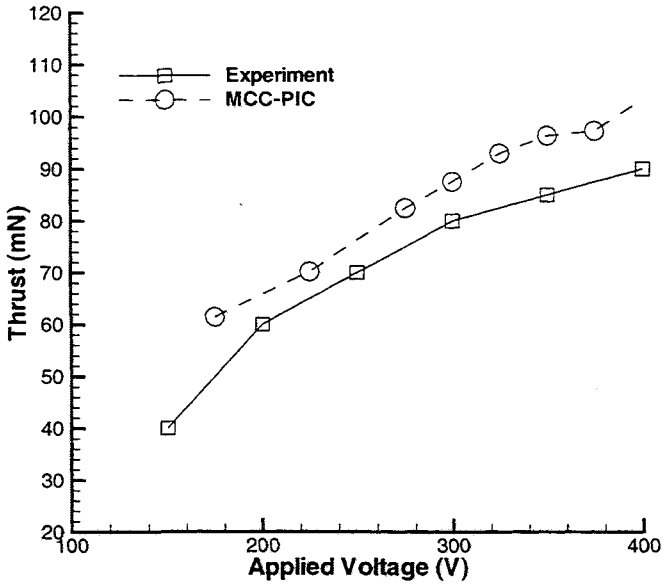

Fig. 7. Time-averaged thrust as a function of applied voltage at a flow rate of 5 mg/s.

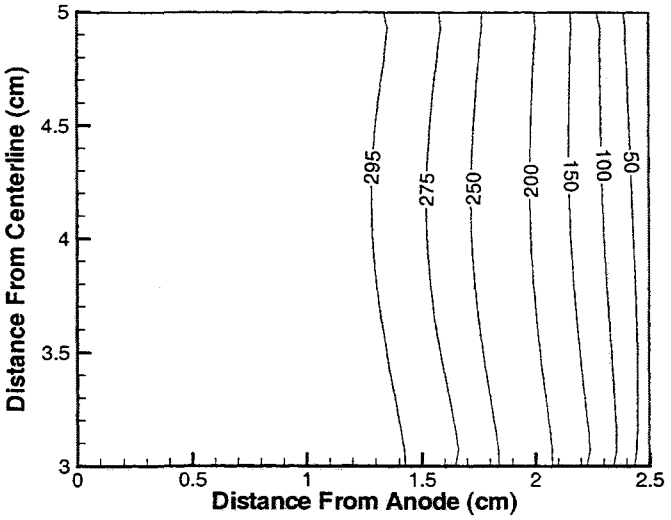

Fig. 8. Time-averaged plasma potential (Volts) for an applied voltage of 300 V.

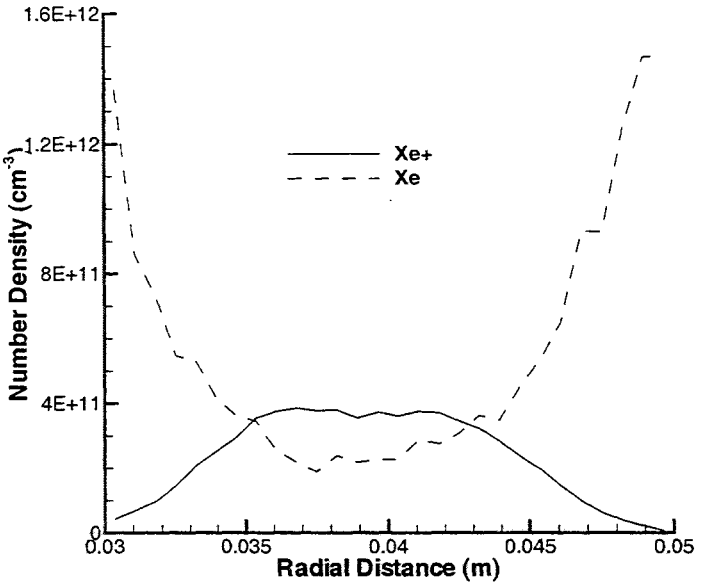

Fig. 9a. Number densities across the thruster exit from time-averaged velocity distribution functions.

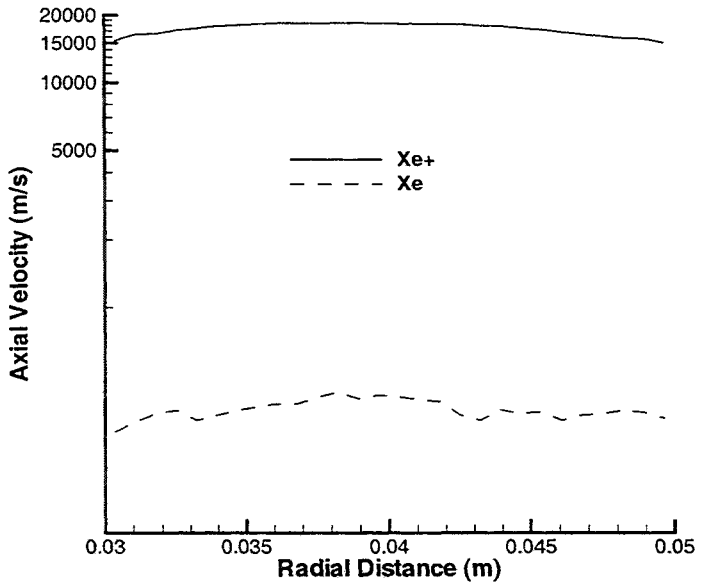

Fig. 9b. Axial velocities across the thruster exit from time-averaged velocity distribution functions.

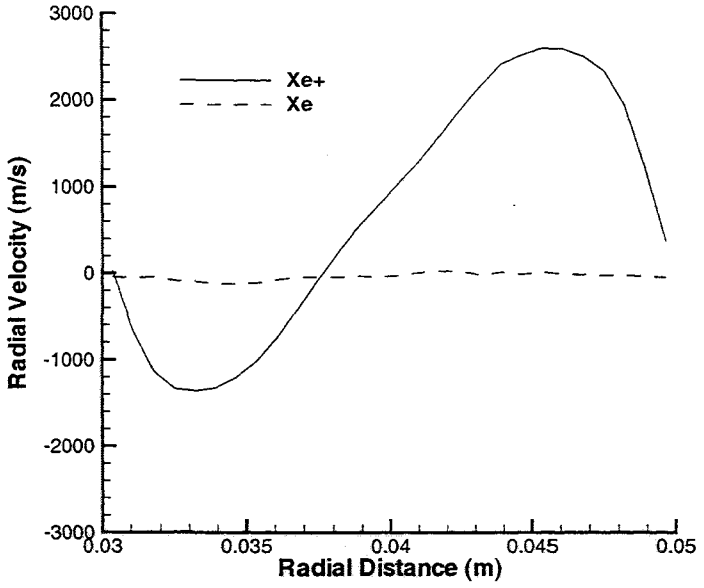

Fig. 9c. Radial velocities across the thruster exit from time-averaged velocity distribution functions.

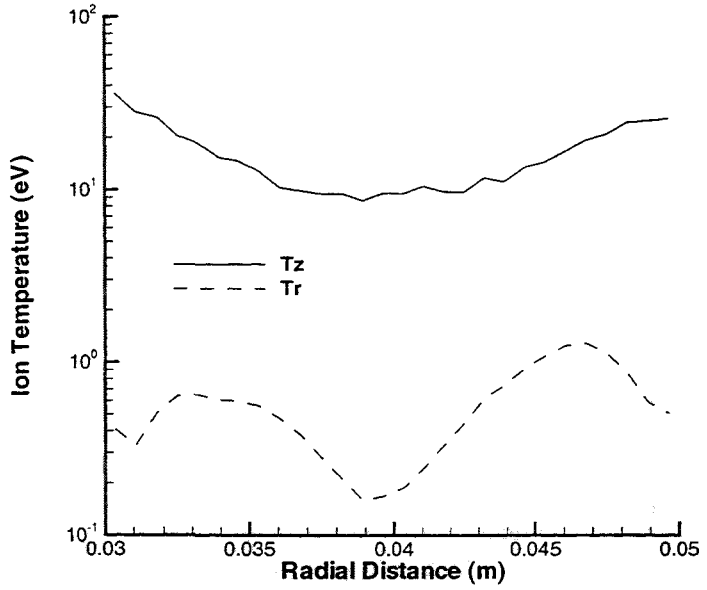

Fig. 9d. Axial and radial temperatures across the thruster exit from time-averaged velocity distribution functions.

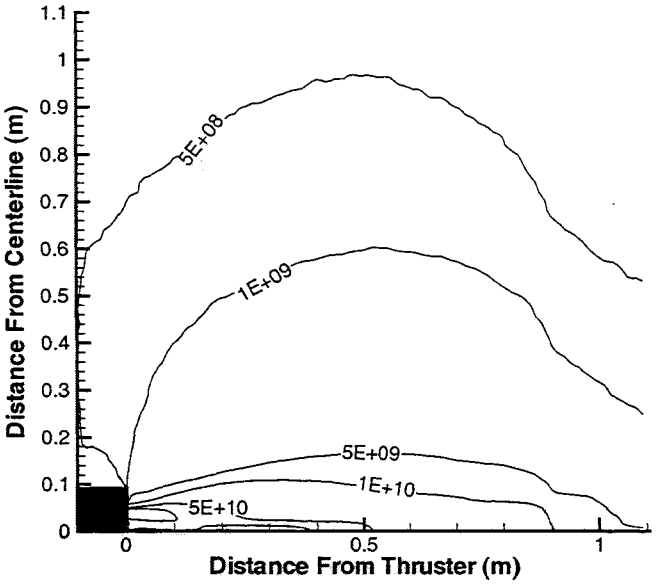

Fig. 10. Contours of ion density (cm^{-3}) in the plume of the SPT-100.

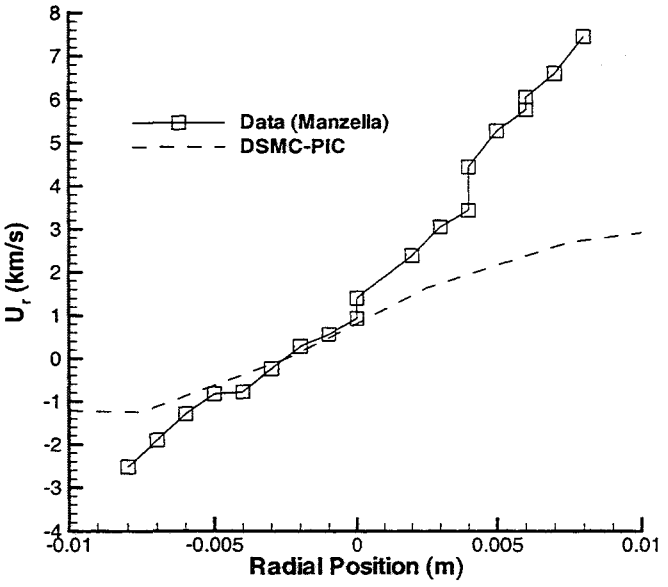

Fig. 11. Radial profile of radial ion velocity component at 11 mm from the thruster exit.

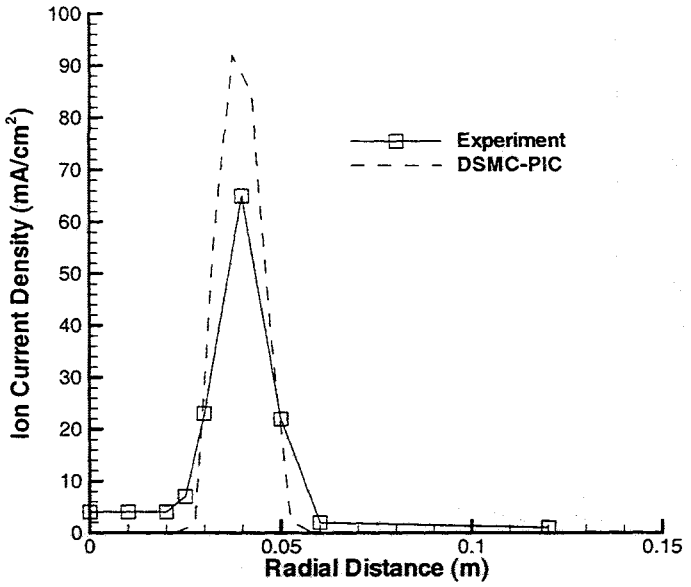

Fig. 12a. Radial profile of ion current density at 10 mm from the thruster.

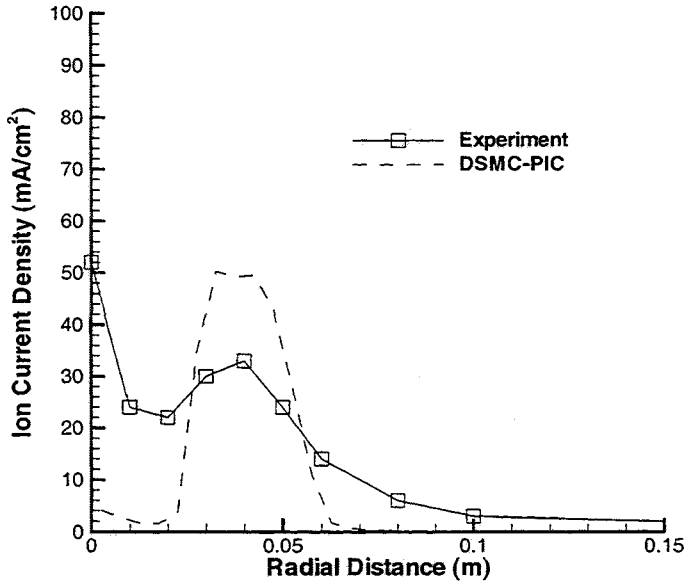

Fig. 12b. Radial profile of ion current density at 50 mm from the thruster.

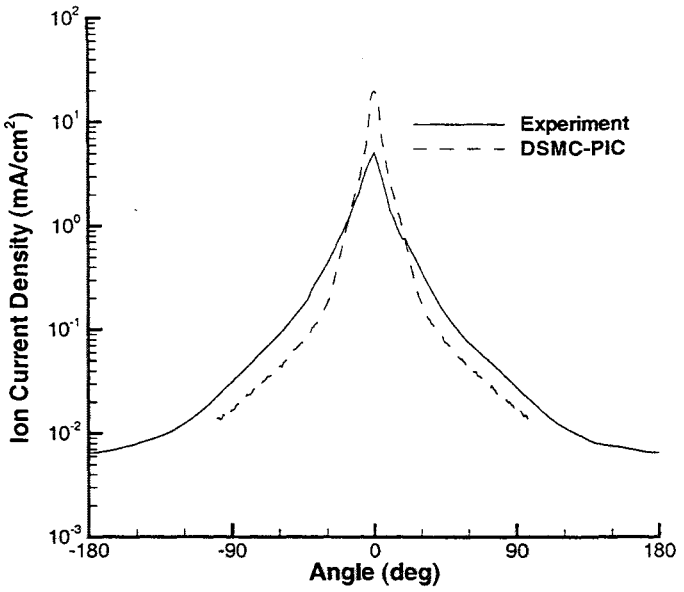

Fig. 13a. Angular profile of ion current density at 50 cm from the thruster.

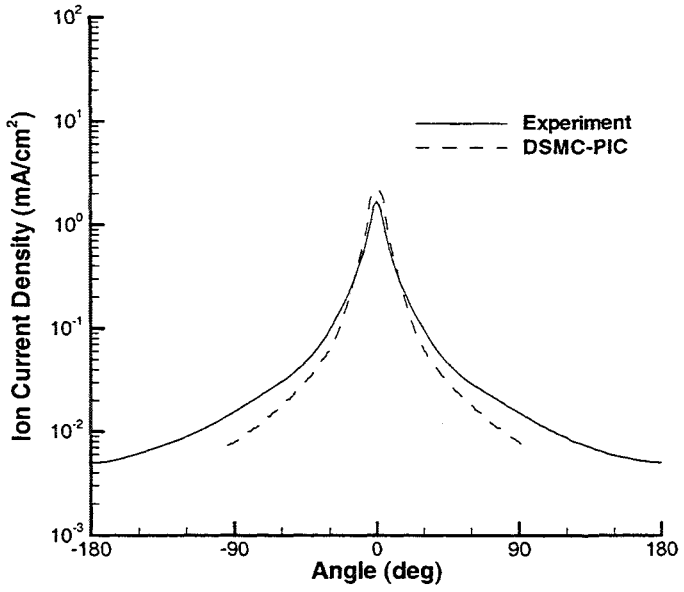

Fig. 13b. Angular profile of ion current density at 100 cm from the thruster.

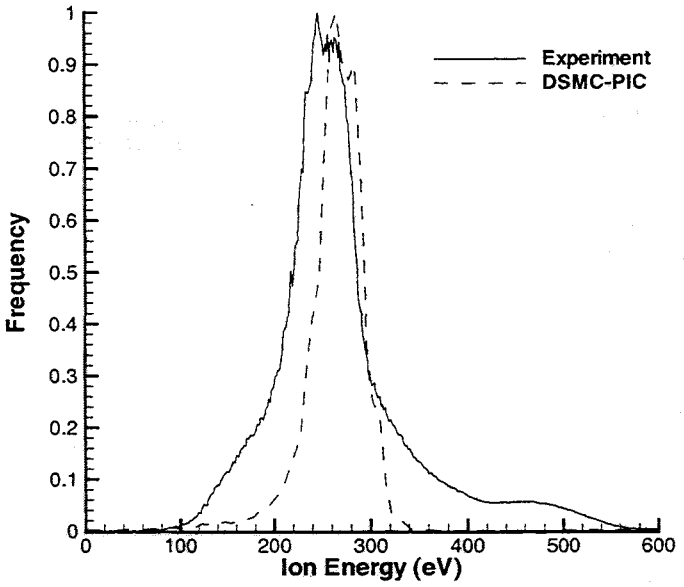

Fig. 14. Ion energy distribution on the plume axis at 50 cm from the thruster.